ADVANCED MATERIALS
www.advmat.de

Intrinsically Stretchable Biphasic (Solid–Liquid) Thin Metal Films

*Arthur Hirsch, Hadrien O. Michaud, Aaron P. Gerratt, Séverine de Mulatier, and Stéphanie P. Lacour**

Stretchable conductors are the foundation of soft electronic circuits.[1] Manufacturing elastic wiring networks to distribute and carry electrical potentials and currents in soft circuits is a persistent challenge, as micrometer-scale structuring over large areas, high electrical conductivity, robustness, long-term stability, and reliable mechanical performance are rarely concurrent.[2] In the last decade, combinations of materials and manufacturing techniques have been proposed to engineer stretchable conductors and related networks. We distinguish two classes of stretchable electronic conductors based on solid and liquid materials. There is also potential for ionic conductors to be implemented as stretchable conductors, but they currently apply only to selected applications.[3]

The stretchability of solid electronic conductors is enabled, but also limited by, geometric designs engineered at the nano-, micro-, and macroscopic scales. Meanders are a straightforward design leading to reversible elasticity. Nearly constant electrical resistance is maintained independently of applied elongation in conductors with wrinkles induced by prestretching of the elastomeric substrate,[4] or buckling of plastic–metal–plastic multilayered ribbons.[1b,5] The integration of these constructs on soft substrates may be complex, and the engineered elasticity is usually limited to predefined directions. Microstructuring and nanostructuring of thin metal films embedded in elastomeric substrates are efficient strain relief approaches enabling reversible, multiaxial stretchability to tens of percent.[1e,6] These conductors display electrical conductivity much lower than continuous metal films of similar thickness. Composites prepared with nanomaterials, e.g., carbon nanotubes, metallic nanowires and nanoparticles, embedded in elastomeric carriers are a popular alternative as they enable tailored, multiaxial elastic conductors but associated patterning and contacting techniques are challenging.[7]

The second class of stretchable electronic conductors employs liquids as conductive materials. Liquids flow "on demand" and rearrange under the influence of external forces. Liquid metals, encapsulated in soft materials, have therefore attracted much attention in recent years[2a,8] to manufacture soft conductors with metallic conductivity, high stretchability and reconfigurability.[9] Gallium-based alloys, rather than toxic mercury, are widely used. The high surface tension and the passivating oxide skin that spontaneously forms on the surface of these liquids hinder their patterning using conventional techniques. Alternative methods focus on injection into channels, molding and printing for rapid manufacturing of highly conductive and stretchable metal networks but none of these patterning techniques offer high-resolution batch processing over large (wafer-scale) surface areas.[10]

Based on these observations, we developed a new class of stretchable electronic conductors formed of biphasic solid–liquid thin metal films. A bilayer metallization sequence starting with the sputtering of an alloying gold film followed by the thermal evaporation of liquid gallium (that displays a melting point of 29.8 °C[11]) results in a heterogeneous film composed of clusters of the solid intermetallic alloy $AuGa_2$ and supercool liquid gallium forming a continuous network and dispersed bulges[11b,12] (**Figure 1**a–c). We designed and engineered the biphasic metallic films to be compatible with large-area and standard microfabrication. Figure 1d,e shows examples of fine patterns produced at wafer scale on elastomeric substrates. Multilayered stretchable circuits can be readily integrated by covalently bonding membranes hosting patterned biphasic conductors connected through soft vias. Figure 1e displays a 4×4 wafer-sized hybrid array of surface mounted light emitting diodes interconnected with a two-level network of biphasic solid–liquid conductors. The array withstood demanding multiaxial inflation cycles, constantly delivering power to the optoelectronic devices (Movie S1, Supporting Information).

To prepare the stretchable biphasic solid–liquid thin metal films, a two-step process was developed in which liquid gallium was evaporated on a substrate preliminarily coated with a wetting and alloying thin film. We selected poly(dimethylsiloxane) (PDMS), a silicone, as the soft carrier substrate and a gold film sputtered on the PDMS as the alloying layer. However, our process is not limited to those materials (Figure S1 and S2, Supporting Information). Non-noble metals may be used, provided the alloying thin film is not oxidized.

The high surface tension of the liquid metal prevented the formation of an evaporated continuous liquid metal film on bare silicone substrates. Instead, the surface of the elastomer was covered with a nonconducting arrangement of liquid gallium microdroplets (Figure S3, Supporting Information). In contrast, evaporating gallium on an alloying metal film, first deposited on the silicone surface, overcame the cohesive forces

A. Hirsch, H. O. Michaud, Dr. A. P. Gerratt, S. de Mulatier, Prof. S. P. Lacour
Bertarelli Foundation Chair in Neuroprosthetic Technology
Laboratory for Soft Bioelectronic Interfaces
Institute of Microengineering
Institute of Bioengineering
Centre for Neuroprosthetics
École Polytechnique Fédérale de Lausanne (EPFL)
1015 Lausanne, Switzerland
E-mail: stephanie.lacour@epfl.ch

DOI: 10.1002/adma.201506234

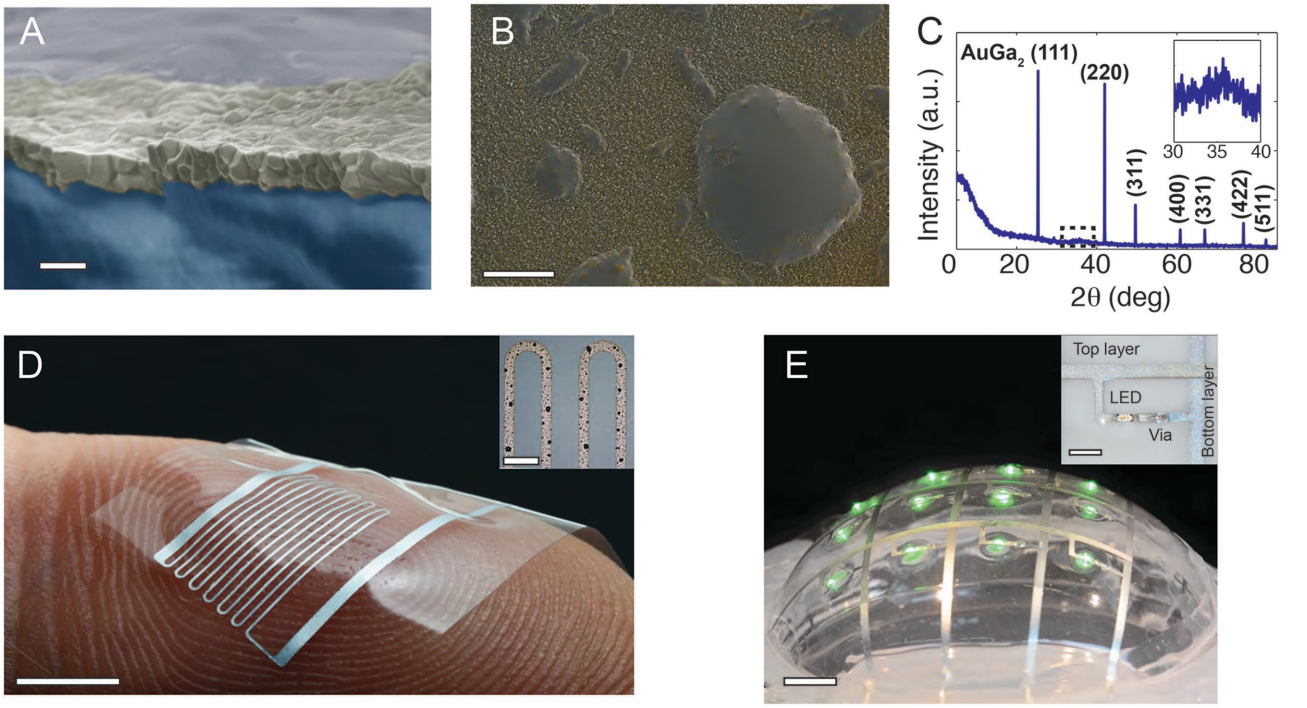

Figure 1. Intrinsically stretchable biphasic gold–gallium thin films. A) False color scanning electronic microscopy (SEM) image of a slightly tilted cross-section of the biphasic gold–gallium film on a PDMS substrate. The blue, yellow and gray colors correspond to the PDMS substrate, the biphasic $AuGa_2$/Ga film, and a gallium bulge in the background, respectively. Scale bar: 500 nm. B) False color SEM image of the surface of the biphasic gold–gallium film. The yellow and gray colors correspond to the $AuGa_2$/Ga film and the liquid Gallium, respectively. Color mask was obtained from backscattered electron detector (BSE) image. Scale bar: 5 μm. C) X-ray diffraction pattern of a biphasic gold–gallium film deposited on a PDMS substrate clearly indicating the position of the peaks corresponding to $AuGa_2$ intermetallic compound (ICDD PDF Card 01-072-5268). Inset: the increase in baseline signal around 35° is attributed to liquid gallium. D) Picture of a biphasic gold–gallium film patterned by photolithography with critical dimension of 100 μm on a 40 μm thick poly(dimethylsiloxane) (PDMS) elastomer membrane. Scale bar: 5 mm; Inset scale bar: 500 μm. E) Stretchable multilayered matrix of green surface mounted light emitting diodes interconnected and powered through biphasic gold–gallium conductors. Scale bar: 15 mm. Inset: the LEDs are interconnected with two biphasic conductor planes; scale bar: 2 mm.

by allowing the liquid metal to diffuse, which further promoted the development of a continuous biphasic thin film.

To assess the growth of the gold–gallium solid–liquid films and the transition from a solid to a biphasic material, we analyzed their surface with scanning electron and atomic force microscopies (**Figure 2**). We defined the parameter β as the atomic ratio (n_{Ga}/n_{Au}) in the biphasic film (see Figure S4 in the Supporting Information). Before gallium evaporation, $\beta = 0$. The gold-coated PDMS surface revealed characteristic wrinkles resulting from compressive stress induced by thermal expansion of the elastomeric substrate during deposition of the solid metal film.[13] For $\beta = 3.2$, pronounced buckling with micrometer amplitude and wavelength was observed. The gold film completely alloyed with the evaporated gallium to form the intermetallic compound $AuGa_2$ (Figure S5 and S6, Supporting Information). Gold–gallium alloying results in large volume expansion (340%) of the film as the lattice constant of the metal increases from 4.08 Å in pure gold to 6.08 Å in $AuGa_2$.[11a] This likely induces larger compressive stress in the thin film on the PDMS substrate, reinforcing its wavy topography (Figure 2c). As the ratio was increased further ($\beta = 3.9$), the buckling in the film disappeared. This was also concomitant to accumulation of liquid gallium in microscopic bulges of different sizes (<1 μm) (Figure 2). Adding more gallium resulted in a distribution of larger bulges (<20 μm for $\beta = 13$) while the rest of the $AuGa_2$/Ga film remained flat. In films prepared with very high β ($\beta = 26$), more than 80% of the film surface area remained thin (<1 μm thick) (Figure S7, Supporting Information).

We next evaluated the electromechanical performance of the biphasic solid–liquid film on PDMS substrates. We characterized the biphasic conductors during uniaxial stretching cycles with four-wire resistance measurements and scanning electron microscopy (**Figure 3**; Figure S8, Supporting Information). Films prepared with $\beta < 3.2$ were conductive after fabrication but failed with catastrophic cracking during release from the carrier substrate and subsequent handling. For $\beta = 3.9$, the films maintained electrical conduction when strained up to 0.8. For large deformations (strain > 0.1), the amount of liquid gallium available was not sufficient to prevent the formation of cracks thereby leading to irreversible damage in the film and permanent degradation of its macroscopic electrical conductivity (Figure 3a,b). Scanning electron microscopy images suggest the biphasic film coped with the applied deformation by maintaining partial continuity. In films prepared with $\beta > 6$, liquid gallium percolated throughout the $AuGa_2$ clusters and maintained electrical continuity in the tested strain range (0–0.8 strain) (Figure 3a,b; Figure S9, Supporting Information).

Adv. Mater. **2016**,
DOI: 10.1002/adma.201506234

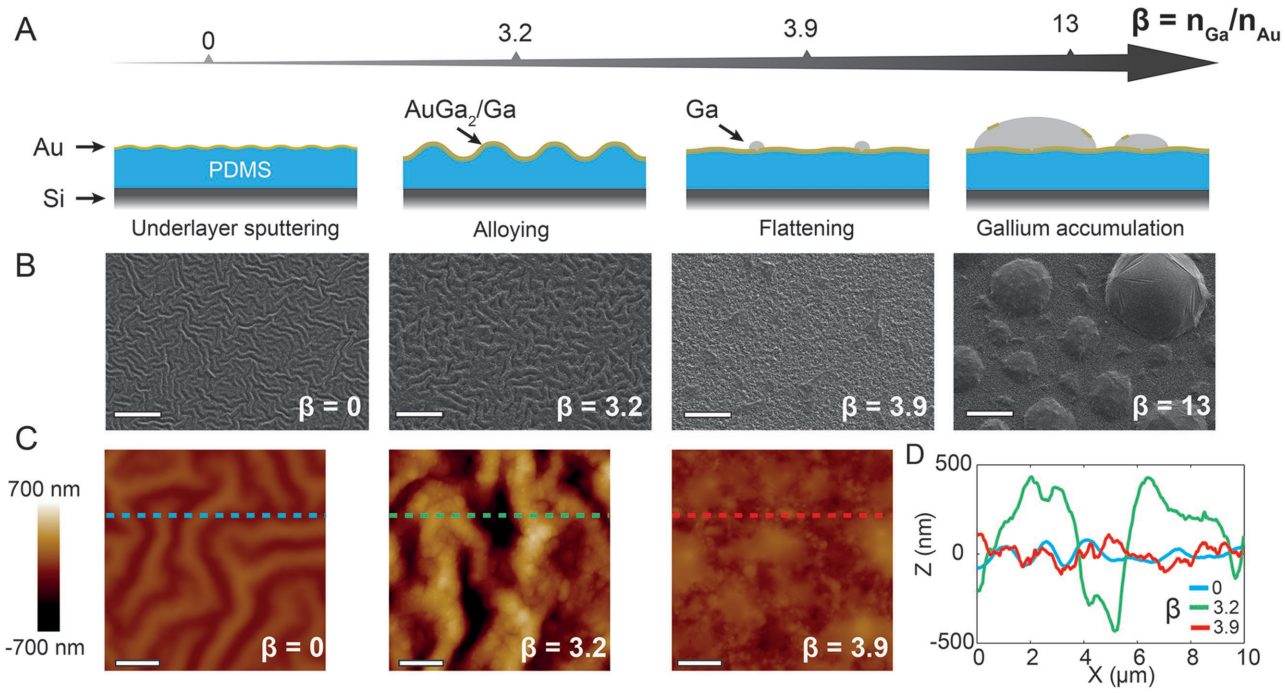

Figure 2. Growth of biphasic gold–gallium thin films on a PDMS membrane. A) Schematic representations of the growth of the biphasic film on a PDMS substrate as a function of the gallium/gold atomic ratio, β. The PDMS substrate was first coated with a 60 nm thick film of sputtered gold. Gallium was then deposited by thermal evaporation. At $\beta = 3.2$, gallium alloyed with gold to form the $AuGa_2$ intermetallic compound; an increased roughness was observed. At $\beta = 3.9$, the film flattened and micrometer-sized gallium accumulations appeared at the surface of the film. At $\beta = 13$, additional gallium further accumulated to form bulges. B,C) SEM and atomic force microscopy (AFM) images of the surface of the biphasic films deposited on PDMS substrates and as a function of increasing β ratio, respectively. SEM scale bars: 10 μm. AFM scale bars: 2 μm. D) Cross-section profiles along the dotted lines indicated on the AFM scans displayed in (C).

Next we assessed the initial sheet resistance, the gauge factor and relative change of resistance at relaxed state (0 strain) after twenty stretching cycles (0–0.5 strain) of the biphasic films (Figure 3c). The sheet resistance is reported assuming that the measurement is made over a length scale much greater than the thickness ($l \gg t$) and topology of the film, which can therefore be considered an electrically homogenous material. We found that for sufficiently high atomic ratios ($\beta > 6$), the biphasic films combined low sheet resistance (<1 Ω sq^{-1}), low gauge factor (≈1), and no dependence on strain history.

In brief, the elemental composition of the biphasic films defines their electromechanical response: a) for $\beta < 3.2$, the film initially conducts and fails at minimal stretch; b) for $3.2 < \beta < 6$, the electrical conduction of the film displays strain-history dependence; c) for $\beta > 6$, the film displays low sheet resistance regardless of the strain history (Figure 3a–c).

To demonstrate the electromechanical robustness and assess fatigue resistance of the biphasic films, we stretched a conductor ($\beta = 13$) to 0.5 strain one million times over a period of 1 week (Figure 3d). The film withstood the cyclic deformation, displaying minimal variation in resistance over time. When processed on a polyurethane substrate, the biphasic metallization ($\beta = 5.2$) sustained reliably uniaxial stretching to five times its initial length (Figure 3e). We radially stretched a PDMS membrane hosting biphasic conductors ($\beta = 13$) to three times its initial surface area. The PDMS membrane fractured before the biphasic conductors electrically failed (Figure S10, Supporting Information).

The physical deposition process also enabled patterning using a conventional and high throughput microstructuring method (Figure 1d and **Figure 4**; Figure S11 and S12, Supporting Information). We developed a scalable lift-off process to achieve a critical dimension of 10 μm (Figure S12a, Supporting Information). There is a tradeoff between high-resolution patterning and high electromechanical performance, i.e., the selection of β should lead to liquid gallium bulges small enough to enable efficient lift-off. We produced arbitrary 2D shapes across an extended area (more than 50 mm × 80 mm) while maintaining sharp features (RMS edge roughness of 2.7 μm for a 10 μm × 15 mm line; see Figure S12b–d in the Supporting Information), and we confirmed the exceptional electromechanical performance of the micropatterned conductive tracks (Figure S13, Supporting Information). Figure 4 illustrates the advanced capabilities of the solid–liquid metallization. We manufactured stretchable optoelectronic circuits, wearable sensors and heaters, and dielectric elastomer actuators. Interconnects and electrodes were exclusively prepared with intrinsically stretchable biphasic metal films.

We fabricated hybrid circuits of light emitted diodes (0.5 mm × 1 mm × 0.2 mm surface mount LEDs) interconnected with biphasic metal film conductors (Figure 1e and 4a). Figure 4a shows characteristic $I - V$ transfer curves for a soft LED microcircuit stretched to 0.8 uniaxial strain.

ADVANCED MATERIALS
www.advmat.de

www.MaterialsViews.com

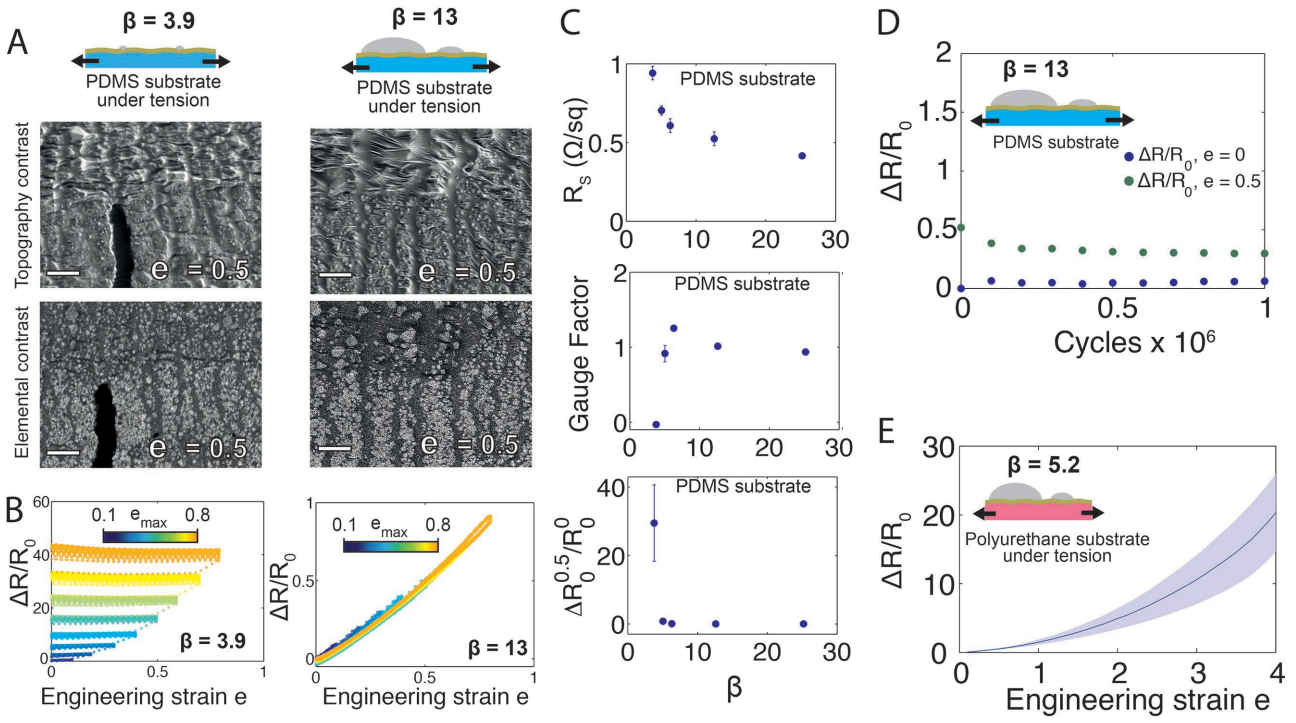

Figure 3. Electromechanical response of biphasic gold–gallium films under large uniaxial deformation. A) SEM images of the surface of biphasic gold–gallium thin films prepared with atomic ratio β of 3.9 and 13 on PDMS substrates. Top and bottom SEM images were obtained with the Everhart–Thornley (ET) detector for topographical contrast, and the backscattered electron (BSE) detector for elemental contrast, respectively. Scale bar: 2 μm. B) Relative change in electrical resistance as a function of applied engineering strain e of biphasic conductive tracks prepared with atomic ratio β of 3.9 (left) and 13 (right). The conductors were first cycled 20 times to 0.1 applied strain. Next, every 20 stretch cycles, the maximal applied strain was increased by 0.1 to reach a maximal strain of 0.8. C) Initial sheet resistance (e = 0), gauge factor (calculated over 0.5 strain cycle), and relative change in electrical resistance (e = 0) after cycling to 0.5 maximum applied strain (n = 3 samples, error bars: S.D.). D) Relative change in electrical resistance over one million cycle to 0.5 strain of a biphasic gold–gallium conductor prepared with the atomic ratio β = 13. E) Relative change in electrical resistance of a biphasic gold–gallium conductor prepared with the atomic ratio β = 13 deposited on a polyurethane substrate. (n = 10 samples, ± S.D.).

The applied stretch minimally impacted the response of the diode circuit.

We prepared flexion-sensing strips composed of two strain gauges and interconnects integrated in a thin PDMS membrane (150 μm total thickness; Figure S14, Supporting Information). The thinness and softness of the sensing strips allowed for direct mounting on human skin and free motion of the fingers. Truly wearable sensors find applications in motion tracking, rehabilitation,[14] and soft robotics.[15] Our soft sensors monitored the full range of motion of the human finger, and the outcome in terms of kinematic reconstruction is comparable to our benchmark motion tracking system (Figure 4b and Figure S15 and Movie S2, Supporting Information).

We combined lift-off micropatterning and multilayer assembly methods to fabricate resistive Joule heaters. The biphasic metal displayed a thermal coefficient of resistance of 1.43×10^{-3} K^{-1} and was compatible with high surface current densities (up to 200 A m^{-1}; Figure S16, Supporting Information). The soft epidermal thermal actuators provided a well-controlled heat source on the skin (Figure 4c), opening opportunities in noninvasive or minimally invasive biomedical mapping.[16]

We also fabricated an electromechanical actuator with a dielectric elastomer sandwiched between soft biphasic electrodes (Figure 4d and Figure S16 and Movie S3, Supporting Information). The tip of the cantilever actuator traced the predicted displacement of voltage-controlled actuation.[17] With a microfabrication-based process, the highly stretchable, highly conductive biphasic electrodes may find substantial use in soft actuation[18] and robotics. Similar constructs may be used for tactile capacitive sensing applications (Movie S4, Supporting Information).

In summary, compared with peer material technologies, biphasic solid–liquid thin gallium-based films answer demands for electrical and mechanical performance as well as patternability and scalability. Key to enabling the distinctive ability to manufacture intrinsically stretchable metallic conductors is the vapor phase deposition of liquid metal on an alloying thin metal film, leading to the formation of a continuous and thin solid–liquid film.

We demonstrated that biphasic solid–liquid thin metal lines can be routed in circuits to transport electrical signals between electronic devices and distribute power, and that they can do so even under demanding repeated and multiaxial mechanical loading. Biphasic solid–liquid conductors offer a promising means to generate useful stretchable devices and circuits. Exploiting the ability to arbitrarily pattern the thin and soft metallization with micrometer-scale precision over large areas will provide opportunities in a range of applications in tactile

DOI: 10.1002/adma.201506234

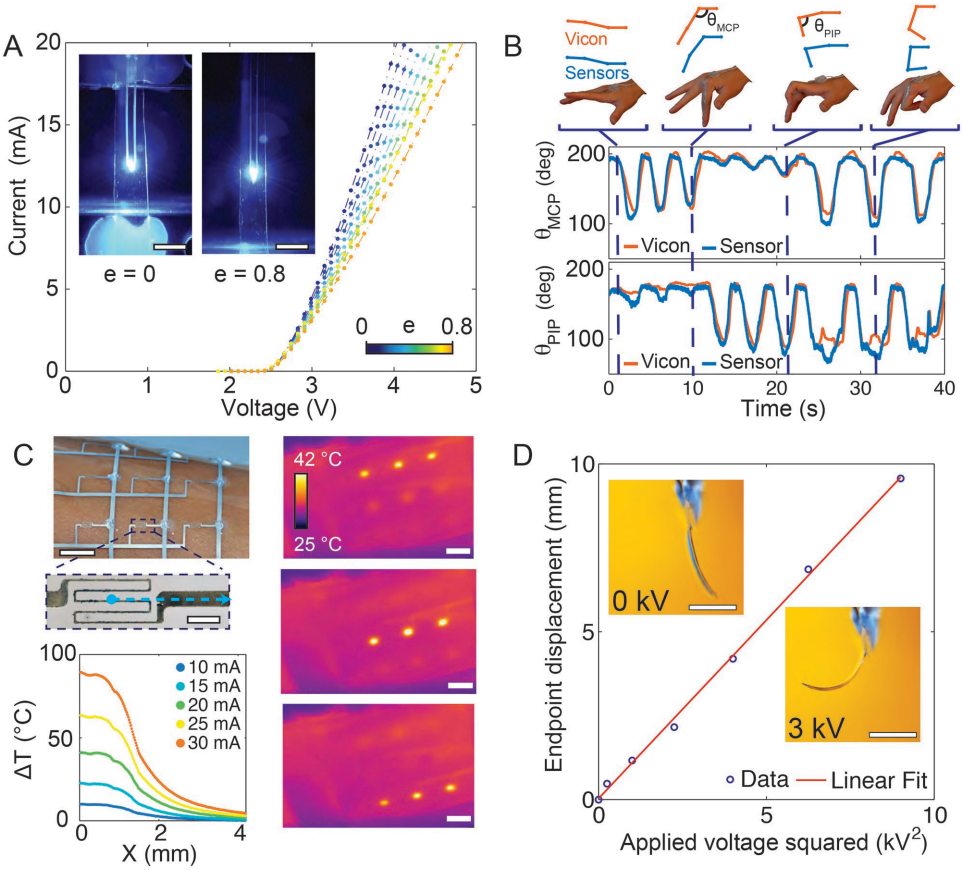

Figure 4. Soft optoelectronic assembly and transducers enabled by intrinsically stretchable biphasic metallization. A) *I–V* characteristics of an SMD LED in PDMS interconnected with biphasic gold–gallium conductors as a function of applied uniaxial strain. Scale bar: 2 mm. B) Epidermal flexion sensor skin monitoring the position of the metacarpophalangeal (MCP) and proximal interphalangeal (PIP) joints of a finger. Joint angles as a function of time monitored by a soft biphasic gold–gallium sensor (blue) and Vicon motion capture system (orange). C) Soft matrix of microheaters wrapped on a human arm. Temperature gradients along the *x*-axis are indicated by the blue arrow. Infrared images of a 3 × 3 matrix of microheaters on the human forearm while sequentially heating one row after the other. Scale bars: 10 mm except for zoomed microheater picture: 1 mm. D) Soft cantilever dielectric elastomer actuator prepared with biphasic gold–gallium electrodes. The actuator is 14 mm long, 1 mm wide and 120 μm thick. Displacement of the end point as a function of the applied voltage squared. Scale bars: 10 mm.

electronic skins, deployable circuits, soft robotics, and soft bioelectronics.

Experimental Section

PDMS Substrate Preparation: First, 4 in. silicon wafers were exposed to oxygen plasma (Harrick Plasma cleaner, 200 mTorr, 29 W, 30 s), then coated with a self-assembled layer of trichloro(1H,1H,2H,2H-perfluorooctyl) silane (Sygma Aldrich) in a dessicator. Poly(dimethylsiloxane) (PDMS) (Sylgard 184, Dow Corning, mixed at 10:1 (w:w), prepolymer:crosslinker) was then spin-coated on the Si wafers (500 RPM for 1 min) and cured at 80 °C for at least 2 h in a convection oven.

Stencil Mask Patterning of Biphasic Gold–Gallium Thin Films: A customized Kapton shadow mask patterned with the negative of the conductor layout was laminated on the PDMS substrate. 60 nm of gold was sputtered through the shadow mask (DP 650, Alliance Concept). Next, a mass of pure gallium ranging from 0.1 to 1 g was thermally evaporated (VACO 250, Vacotec) on the gold-coated substrate. After evaporation, the Kapton mask was delicately peeled off the substrate to form the desired pattern.

Lift-Off Patterning of Biphasic Gold–Gallium Thin Films: A PDMS substrate was exposed to oxygen plasma (200 mTorr, 29 W, 30 s), then spin-coated with photoresist (AZ-9260 from MicroChemicals) at 6000 rpm for 90 s and left at room temperature for 12 h. The resist was then exposed with a 210 mJ cm^{-2} dose (MJB4 mask aligner from Suss MicroTec, 365 nm UV lamp), developed in diluted AZ-400-K (MicroChemicals, 4:1 deionized water to developer volume ratio) and dried for 15 min at 60 °C on a hot plate. 40 nm of gold was sputtered to form an alloying layer and then 0.2 g of gallium was thermally evaporated. Lift-off was performed in a bath of SVC-14 (Shipley) for 24 h, followed by drying at 60 °C on a hot plate for 15 min.

Uniaxial Electromechanical Characterization: Biphasic gold–gallium thin film conductors were stencil-patterned on 120 μm thick PDMS to produce 15 mm long and 0.3 mm wide electrical conductors. Samples were subsequently cut in 10 mm by 30 mm rectangles and peeled from the wafer. Samples were mounted on a custom-built uniaxial tensile stretcher programmed to actuate two clamps moving in opposite directions along the horizontal plane. Each clamp featured two contact pads that provided constant electrical and mechanical contact to the sample under test. The position of the clamps and the electrical resistance of the conductor, measured using a four-point probe method (2400 source-meter, Keithley), were acquired synchronously at 3.8 Hz on a computer running a dedicated LabVIEW program. For fatigue experiments, the stretcher was programmed to perform one million stretch-relaxation cycles (0–0.5 strain at a frequency of 1.4 Hz). Ten times per decade, counting cycles on a logarithmic scale, the stretcher

slowed to 0.14 Hz for five cycles in order to record the position of the clamps and resistance of the sample.

X-Ray Diffraction Analysis: The analysis was conducted in a D8 Discover diffractometer from Bruker, with a Cu K_α radiation ($\lambda = 1.54$ Å, 0.05° steps, 2 s per step). All samples were prepared and scanned on a float glass support wafer.

Scanning Electron Microscopy: SEM images were acquired in a Merlin microscope from Zeiss, using the Everhart–Thornley detector at a beam energy of 2–3 keV for topography contrast, and the backscattered electron detector at beam energy of 2–3 keV and grid voltage of 400 V for compositional contrast.

Atomic Force Microscopy: Atomic force microscope (AFM) images were acquired in a Dimension Fastscan AFM from Bruker with ScanAsyst-Air-HR probes from same supplier.

Manufacturing of Stretchable Circuits: A detailed description of the assembly of the LED arrays, wearable flexion sensors, thermal and dielectric elastomer actuators is provided in the Supporting Information.

Supporting Information

Supporting Information is available from the Wiley Online Library or from the author.

Acknowledgments

A.H. and H.O.M. contributed equally to this work. A.H., H.O.M., and S.P.L. designed the research; A.H., H.O.M., A.P.G., and S.d.M. performed the experiments; A.H., H.O.M., A.P.G., S.d.M., and S.P.L. analyzed the data; and A.H., H.O.M., A.P.G., and S.P.L. wrote the manuscript. Financial support was provided by the Fondation Bertarelli, a Starting Grant from the European Research Council (ERC 259419 ESKIN), nano-tera.ch (20NA_145923 SpineRepair, 20NA_143070 WiseSkin), and the Swiss National Science Foundation through the National Centre of Competence in Research (NCCR) in Robotics. The authors would like to thank M. Coscia and S. Micera for providing access and help in setting up the camera tracking system, R. Nigon and P. Muralt for the X-ray diffraction scans and fruitful discussions, and the EPFL Center for Micronanotechnology (CMi) staff for their technical support.

Received: December 15, 2015
Revised: January 23, 2016
Published online:

[1] a) S. P. Lacour, J. E. Jones, S. Wagner, T. Li, Z. Suo, *Proc. IEEE* **2005**, *93*, 1459; b) J. Vanfleteren, M. Gonzalez, F. Bossuyt, Y.-Y. Hsu, T. Vervust, I. D. Wolf, M. Jablonski, *MRS Bull.* **2012**, *37*, 254; c) S. Xu, Y. Zhang, L. Jia, K. E. Mathewson, K.-I. Jang, J. Kim, H. Fu, X. Huang, P. Chava, R. Wang, S. Bhole, L. Wang, Y. J. Na, Y. Guan, M. Flavin, Z. Han, Y. Huang, J. A. Rogers, *Science* **2014**, *344*, 70; d) M. L. Hammock, A. Chortos, B. C.-K. Tee, J. B.-H. Tok, Z. Bao, *Adv. Mater.* **2013**, *25*, 5997; e) I. R. Minev, P. Musienko, A. Hirsch, Q. Barraud, N. Wenger, E. M. Moraud, J. Gandar, M. Capogrosso, T. Milekovic, L. Asboth, R. F. Torres, N. Vachicouras, Q. Liu, N. Pavlova, S. Duis, A. Larmagnac, J. Voros, S. Micera, Z. Suo, G. Courtine, S. P. Lacour, *Science* **2015**, *347*, 159; f) K. Tybrandt, J. Vörös, *Small* **2015**, *11*, 180.

[2] a) I. D. Joshipura, H. R. Ayers, C. Majidi, M. D. Dickey, *J. Mater. Chem. C* **2015**, *3*, 3834; b) N. Matsuhisa, M. Kaltenbrunner, T. Yokota, H. Jinno, K. Kuribara, T. Sekitani, T. Someya, *Nat. Commun.* **2015**, *6*, 1.

[3] a) J.-B. Chossat, Y.-L. Park, R. J. Wood, V. Duchaine, *IEEE Sens. J.* **2012**, *13*, 3405; b) C. Keplinger, J.-Y. Sun, C. C. Foo, P. Rothemund, G. M. Whitesides, Z. Suo, *Science* **2013**, *341*, 984.

[4] K. S. Kim, Y. Zhao, H. Jang, S. Y. Lee, J. M. Kim, K. S. Kim, J.-H. Ahn, P. Kim, J.-Y. Choi, B. H. Hong, *Nature* **2009**, *457*, 706.

[5] S. Wang, Y. Huang, J. A. Rogers, *IEEE Trans. Compon., Packag., Manuf. Technol.* **2015**, *50*, 1201.

[6] C. F. Guo, Q. Liu, G. Wang, Y. Wang, Z. Shi, Z. Suo, C.-W. Chu, Z. Ren, *Proc. Natl. Acad. Sci. USA* **2015**, *112*, 12332.

[7] a) J. Liang, L. Li, X. Niu, Z. Yu, Q. Pei, *Nat. Photonics* **2013**, *7*, 817; b) Y. Kim, J. Zhu, B. Yeom, M. D. Prima, X. Su, J.-G. Kim, S. J. Yoo, C. Uher, N. A. Kotov, *Nature* **2013**, *500*, 59; c) M. Park, J. Park, U. Jeong, *Nano Today* **2014**, *9*, 244.

[8] a) M. D. Dickey, R. C. Chiechi, R. J. Larsen, E. A. Weiss, D. A. Weitz, G. M. Whitesides, *Adv. Funct. Mater.* **2008**, *18*, 1097; b) B. Kim, J. Jang, I. You, J. Park, S. Shin, G. Jeon, J. K. Kim, U. Jeong, *ACS Appl. Mater Interfaces* **2015**, *7*, 7920.

[9] E. Palleau, S. Reece, S. C. Desai, M. E. Smith, M. D. Dickey, *Adv. Mater.* **2013**, *25*, 1589.

[10] S. Cheng, Z. Wu, P. Hallbjörner, K. Hjort, A. Rydberg, *IEEE Trans. Antennas Propag.* **2009**, *57*, 3765.

[11] a) R. P. Elliott, F. Shunk, *Bull. Alloy Phase Diagrams* **1981**, *2*, 356; b) K. T. Lee, Y. S. Jung, T. Kim, C. H. Kim, J. H. Kim, J. Y. Kwon, S. M. Oh, *Electrochem. Solid-State Lett.* **2008**, *11*, A21.

[12] D. G. Carlson, J. Feder, A. Segmüller, *Phys. Rev. A* **1974**, *9*, 400.

[13] N. Bowden, S. Brittain, A. G. Evans, J. W. Hutchinson, G. M. Whitesides, *Nature* **1998**, *393*, 146.

[14] H. Zhou, H. Hu, *Biomed. Signal Process. Control* **2008**, *3*, 1.

[15] A. P. Gerratt, H. O. Michaud, S. P. Lacour, *Adv. Funct. Mater.* **2015**, *25*, 2287.

[16] R. C. Webb, R. M. Pielak, P. Bastien, J. Ayers, J. Niittynen, J. Kurniawan, M. Manco, A. Lin, N. H. Cho, V. Malyrchuk, G. Balooch, J. A. Rogers, *PLoS One* **2015**, *10*, e0118131.

[17] T. Maleki, G. Chitnis, B. Ziaie, *J. Micromech. Microeng.* **2011**, *21*, 027002.

[18] R. Pelrine, R. Kornbluh, Q. Pei, J. Joseph, *Science* **2000**, *287*, 836.

DOI: 10.1002/adma.201506234